Coupling of Hawaiian volcanoes only during overpressure condition

Manoochehr Shirzaei,[1,2] Thomas R. Walter,[3] and Roland Bürgmann[2]

Received 2 March 2013; revised 11 April 2013; accepted 12 April 2013; published 29 May 2013.

[1] Mauna Loa and Kilauea volcanoes, Hawaii, are thought to be coupled by pore pressure diffusion through an asthenospheric melt layer. However, abundant observations of independent activity of these volcanoes suggest a more complicated relationship. Here we analyze surface deformation data, deep seismicity and gas measurements, to reveal strong coupling of these volcanoes between 2003 and 2008. In early 2005, we find a shift from anticorrelation to correlation of magma-chamber inflation. The shift is preceded by a seismic swarm in the mantle beneath Mauna Loa and accompanied by a large silent slip event beneath the south flank of Kilauea. This suggests that these volcanoes are coupled during mantle-driven surges and that the 2005 silent slip event was triggered by accelerated magma supply at Kilauea. **Citation:** Shirzaei, M., T. R. Walter, and R. Bürgmann (2013), Coupling of Hawaiian volcanoes only during overpressure condition, *Geophys. Res. Lett.*, *40*, 1994–1999, doi:10.1002/grl.50470.

1. Introduction

[2] Volcanoes tend to cluster in space [*Houghton et al*., 1999] and are sometimes observed to erupt within days from each other [*Houghton et al*., 1999; *Siebert et al*., 2010]. This implies that volcanic systems frequently interact or respond to a common external triggering mechanism [*Hill et al*., 2002; *Linde and Sacks*, 1998; *Manga and Brodsky*, 2006; *Walter and Amelung*, 2006]. This highlights the importance of investigating volcanic and tectonic interactions to characterize time-dependent hazards from active volcanoes.

[3] Mauna Loa and Kilauea volcanoes, being among the most active volcanoes worldwide, are spaced ~30 km apart on the Big Island of Hawai`i. The random distribution of eruptions of individual Hawaiian volcanoes in time without any periodicity [*Klein*, 1982] and the lack of substantial subsidence of Kilauea during Mauna Loa's most recent large eruption in 1984 [*Lockwood et al*., 1985] suggest that these volcanoes are fed by independent magma supply systems. In contrast, observations of alternating magma supply to Kilauea and Mauna Loa [*Klein*, 1982] and of simultaneous inflation at Kilauea and Mauna Loa in 2002 [*Miklius and Cervelli*, 2003] suggest coupling of these two volcanoes, possibly at the asthenospheric level [*Gonnermann et al*., 2012]. These contradictory observations may indicate that these volcanoes are only coupled under certain conditions.

[4] To improve our understanding of correlated behavior of the Hawaiian volcanoes, we investigate Hawaii's time-dependent deformation field using multitemporal InSAR (interferometric synthetic aperture radar) and time-dependent inverse modeling. For this study, we utilized 27 radar images acquired between 2003 and 2008 by the European environmental satellite Envisat. During this period, the magma supply to Kilauea increased by a factor of 2 [*Poland et al*., 2012], and Mauna Loa and Kilauea simultaneously inflated (Figure 1). Given the time series of the surface deformation, we apply a time-dependent inverse modeling scheme to characterize the evolution of the magmatic and tectonic sources at Hawaii. The results of this analysis and modeling provide new insights into the spatial and temporal interaction of Mauna Loa and Kilauea magmatic systems.

2. Methods

[5] We provide a short summary of the methods used, which includes InSAR time series and time-dependent source modeling. These methods are based on previously established works cited below, which provide more detailed information.

2.1. InSAR Time Series

[6] To generate the time series of the surface deformation, we employ a multiple-master SAR interferometry approach [*Shirzaei*, 2013]. Given 27 images acquired in descending orbit of the Envisat satellite (Figure S1 in the auxiliary material), from 2003 to 2008, we generated 173 interferograms with perpendicular and temporal baselines smaller than 600 m and 3 years. The geometrical phase is estimated and subtracted using satellite precise ephemeris data and a Shuttle Radar Topography Mission digital elevation model of 90 m resolution [*Franceschetti and Lanari*, 1999]. To obtain an unambiguous range displacement observation from modulo 2π phase change measured in each interferogram, we use a 2-D phase unwrapping operator [*Chen and Zebker*, 2001]. This operator is applied to a sparse network of stable pixels [*Costantini and Rosen*, 1999]. For details on the pixel selection, see *Shirzaei* [2013]. The effect of satellite orbital error in each unwrapped interferogram is reduced following the method proposed by *Shirzaei and Walter* [2011]. We also corrected every interferogram for spatially correlated components of the atmospheric delay [*Shirzaei and Bürgmann*, 2012]. Then, this data set is inverted using a linear unbiased estimation approach [*Bjerhammar*, 1973] to generate a time series of the surface deformation over the Big Island. High-pass filtering in space and low-pass filtering in time are applied

Additional supporting information may be found in the online version of this article.

[1]School of Earth and Space Exploration, Arizona State University, Tempe, Arizona, USA.
[2]Department of Earth and Planetary Science, University of California, Berkeley, Berkeley, California, USA.
[3]Department 2: Physics of the Earth, GFZ German Research Centre for Geosciences, Potsdam, Germany.

Corresponding author: M. Shirzaei, School of Earth and Space Exploration, Arizona State University, Tempe, AZ 85287-6004, USA. (shirzaei@asu.edu)

0094-8276/13/10.1002/grl.50470

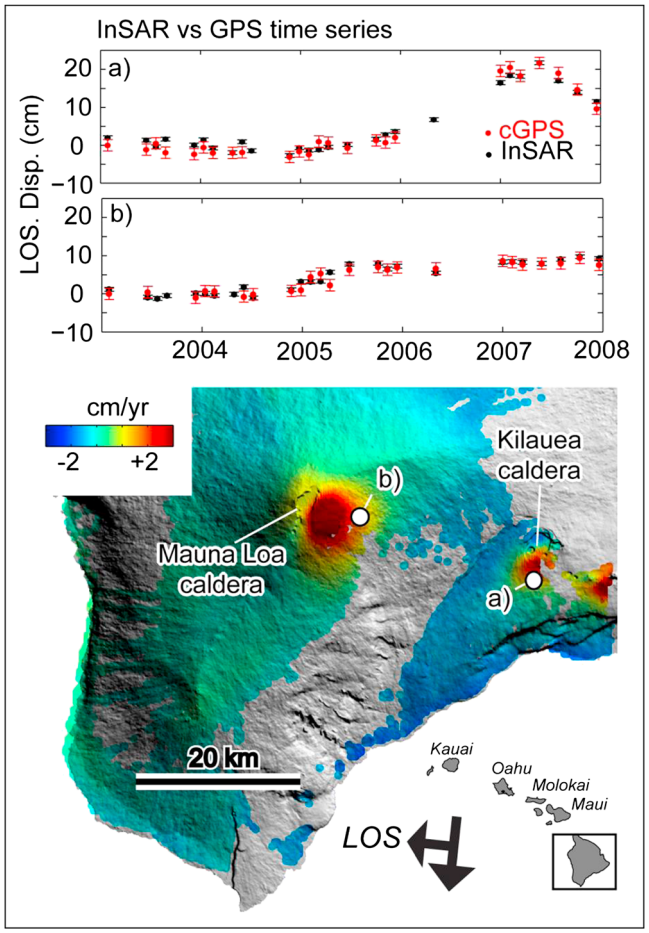

Figure 1. The deformation of the Hawai`i Island as seen from space. The map shows the average velocity in the line of sight to the Envisat satellite for the period 2003–2008. The warmer colors show movement of the ground towards the satellite. The satellite is on a descending orbit path (azimuth ~188°, incidence angle ~23°). Comparison of InSAR time series and cGPS measurements at (a) Kilauea and (b) Mauna Loa, respectively (locations shown by white circles on map). All of the error bars reflect a 95% confidence level.

to reduce the atmospheric delay. The line-of-sight (LOS) velocity of each pixel is estimated as the slope of a best fitting line to the displacement time series using a robust regression approach. Note that since the deformation history is fully nonlinear, the velocity map (Figure 1) is only used for presentation purposes.

2.2. Time-Dependent Source Modeling

[7] To understand the causes of the observed deformation, we developed a time-dependent nonlinear inverse model simulation. This method consists of two main operators: (1) a nonlinear inversion method, genetic algorithm (GA), as a minimum spatial mean error estimator of the source geometry and source parameters [*Shirzaei and Walter*, 2009]; and (2) a recursive filter, Kalman filter (KF), to generate time series of the deformation source parameters as a minimum temporal mean square error estimator [*Grewal and Andrews*, 2001]. These two operators are combined in an iterative manner [*Shirzaei and Walter*, 2010]. By using GA, we solve for the deformation source parameters that reproduce the observed LOS displacement at each time step. Due to the temporal noise of the observations, the source parameters may fluctuate unreasonably in time. To minimize these undulations, we use the KF, which allows for reducing the temporal noise.

[8] To relate the observed displacement field to the volcanic and tectonic sources, we employ the described inverse modeling scheme and use a mathematical model that comprises an analytical solution of rectangular dislocation planes [*Okada*, 1985] and of pressurized spherical sources [*McTigue*, 1987] in an elastic half-space. The initial geometry of the deformation sources is chosen following earlier works (Figure S4). The Mauna Loa system comprises three rift zone segments and a magma chamber, simulated by rectangular dislocations and a pressurized source, respectively, similar to that of *Amelung et al.* [2007]. *Amelung et al.* [2007] simulated only the central rift zone using a single vertical plane, while we added two more rectangular planes attached at the north and south to model the possible curved rift geometry and rift activity along these two branches. During the optimization, we allow for independent opening of each of these three patches. In plan view, the position of the rift zone was defined by geological maps and the depth was free in a range of 14 km to the surface and solved independently for all three rift zone segments. For more details on the model initialization, see Table S1.

[9] The sources of deformation at Kilauea volcano include the southwest and east rift zones, a magma chamber below the summit caldera, and a basal décollement under the south flank of the volcano. The inflation of the magma chamber is simulated using a spherical pressurized source similar to earlier work [*Desmarais and Segall*, 2007]. The intrusions of Kilauea's rift zones are simulated by using rectangular dislocation planes with opening-mode displacement discontinuities, and the décollement is represented by a subhorizontal dislocation with in-plane slip [*Montgomery-Brown et al.*, 2010]. We refer to the Kilauea magma chamber as the reservoir under the Kilauea summit caldera. To speed up the convergence rate of the optimization algorithm and avoid unreasonable solutions, we impose some constraints on the dislocation source parameters as reported in Table S1. These constraints are integrated in the inversion algorithm as bounds for optimization parameters; i.e., the accepted solution should fall within the specified range.

3. Deformation Time Series and Model Results

[10] The InSAR LOS velocity field (Figure 1) and spatio-temporal displacement maps (Figure S2) show deformation at rates of >3 cm/yr over both Kilauea and Mauna Loa. A prominent feature of the surface deformation is that early in 2005, Mauna Loa began a phase of inflation that produced a maximum of 25 cm LOS decrease by mid-2007. After ~1 year of delay, Kilauea started its accelerated inflation exceeding that of Mauna Loa. We compare the InSAR data to GPS (see the auxiliary material for GPS data processing) observations of the surface deformation, which show excellent agreement when the GPS time series is projected onto the satellite LOS (Figures 1a, 1b, and S3).

[11] To understand the underlying causes of this correlated deformation, we employ the time-dependent nonlinear inverse model simulation and the initial source geometries described in section 2.2. To ensure that the trade-off between the Kilauea and Mauna Loa systems does not affect the results, we divided the deformation data into two subsets covering Mauna Loa and Kilauea and run the inversion individually for each set. By inverting for the strength (volume-change/opening/slip) and geometry parameters (depth/width/dip) of the sources within their respective bounds (Table S1) as a function of time, the measured displacement can be reproduced with a root mean square error better than 0.5 cm (Figure S6). The observed surface deformation is best explained by the inflating magma chambers at Mauna Loa and Kilauea located at 4 ± 0.75 km and 3.8 ± 0.75 km below the surface, respectively, the opening of the rift zones at a depth between 1 and 10 ± 2 km (except the Kilauea eastern rift where the opening reaches the surface), and the movement of Kilauea's south flank from slip along a basal décollement located at an average depth of 10 ± 1 km, consistent with deformation sources inferred in earlier studies [*Amelung et al.*, 2007; *Baker and Amelung*, 2012; *Brooks et al.*, 2008; *Montgomery-Brown et al.*, 2009; *Myer et al.*, 2008; *Okubo et al.*, 1997; *Owen et al.*, 2000; *Segall et al.*, 2006]. During 2003–2008, the dominant magmatic activity is observed at the Kilauea rift zone with >0.3 km^3 intruded material. The total volume of intruded magma in Kilauea's rift zone is ~20 times that of the Mauna Loa rift, while the volume increase of the magma chamber at Mauna Loa during this time span is ~4 times larger than that of Kilauea.

[12] The time series of the model source strengths reveals significant temporal variations (Figure S5). At the Mauna Loa rift zone, large fluctuations in the volume flux were found, including both opening (2005–2006) and contraction (2006–2007), while the Mauna Loa magma chamber displayed nearly linear inflation. Kilauea's rift zones show a continuous increase of opening with short-term fluctuations throughout the entire period. Kilauea's magma chamber experienced rapid inflation from mid-2006 until 2007, when it begins an episode of gradual deflation following the June 2007 Kilauea east rift zone intrusion [*Montgomery-Brown et al.*, 2010]. We note that the volume change due to the June 2007 event does not stand out in the Kilauea rift zone strength time series, because its size (2.3×10^7 m^3) is small compared to that of the entire rift. However, the estimated value is in good agreement with the result from earlier works [see *Montgomery-Brown et al.*, 2011].

4. Discussion and Conclusions

[13] We presented the spatiotemporal map of the surface deformation field and a time-dependent model of the underlying deformation sources at Hawaii. In the following, we investigate and interpret the correlated behavior of these sources.

[14] Bivariate plots (Figure 2) illustrate the correlations between the various dislocation sources. For instance, an increasing trend with time means that the correlation is positive (e.g., the magma volume is increasing at both sources), whereas a negative trend indicates an anticorrelation (e.g., the volume of one system is increasing, whereas that of the other system is decreasing). Figure 2 highlights two distinct episodes of anticorrelation (2003–2005) and correlation

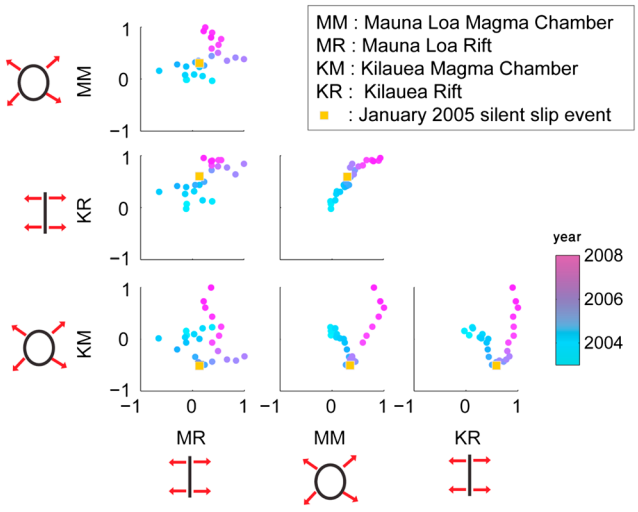

Figure 2. Bivariate plots. This shows the correlation between the strengths of the model sources as a function of time and illustrates the degree and pattern of the relationship. The coordinates of each point represent the values of the normalized volume change associated with two of the magma chamber or rift intrusion sources. We use a color scale to assign a date to each point. In each panel, the image acquired immediately after the silent slip event (31 January 2005) is marked by a yellow square.

(2006–2008) between the magma chambers of Kilauea and Mauna Loa and between Kilauea's magma chamber and its rift zone. We note that during the transition from anticorrelation to correlation, a silent slip event (SSE) occurred on the basal décollement underlying Kilauea's south flank in January of 2005 [*Segall et al.*, 2006]. However, we are not able to resolve the source of this short slip episode. Figures 3a and 3b show the time series of the volume change of the corresponding volcanic sources. Over the period 2003–2005, the volume of Kilauea's magma chamber contracted by ~0.007 km^3. From late 2005, gradual inflation started and culminated in mid-2007 when the volume change of the chamber since the 2005 SSE reached ~0.008 km^3. At this point and following the June 2007 eastern Kilauea rift intrusion [*Brooks et al.*, 2008; *Montgomery-Brown et al.*, 2010], there was gradual deflation. Given the density of 2800–3100 kg/m^3 for solidified gabbro [*Moore*, 2001] and the density of 2600 kg/m^3 for basaltic melts [*Fujii and Kushiro*, 1977] at Kilauea, the solidification causes an ~7–16% volume reduction [*Sigmundsson et al.*, 1997]. Though we cannot discount the contribution of magma cooling and migration to the rift vent, the solidification may explain most of the observed subsidence signal.

[15] The time series of Kilauea rift zone opening (Figure 3a) shows an anticorrelation with the magma chamber volume changes, over the period 2003–2005. From early 2005, both show a similar deformation pattern; i.e., the magma chamber inflation is accompanied by rift opening. However, short episodes of anticorrelated volume changes are evident, typically lasting only for a few months. This suggests that in the years following 2005, although the rift zone and magma chamber compete for supply, the accelerated intrusion of material from the deep reservoir dominates the

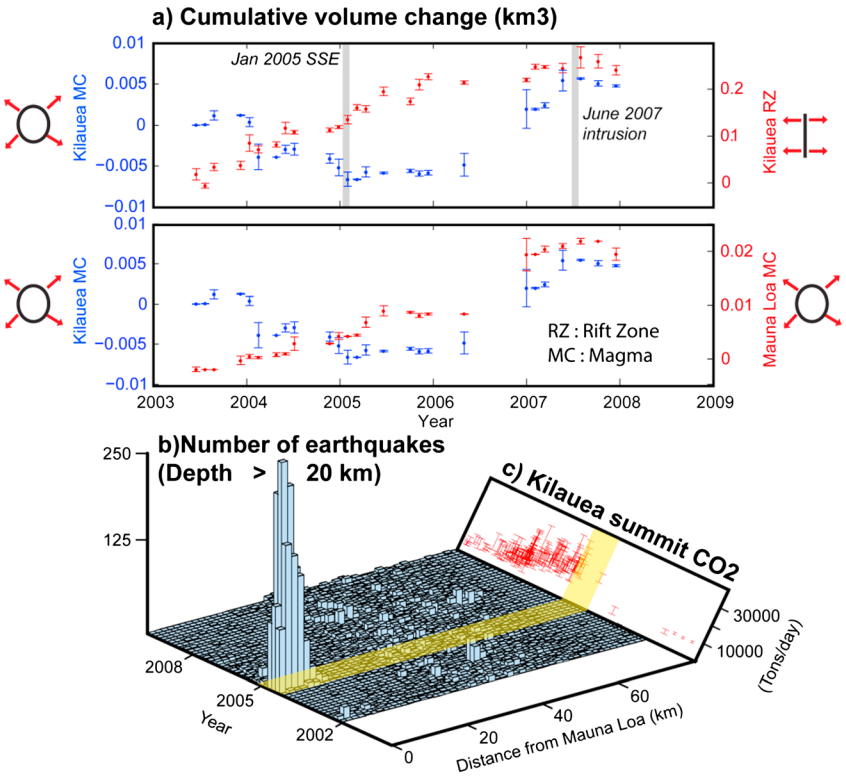

Figure 3. Data and model correlation from surface to depth. (a) Time series of the cumulative volume change in the magma chambers and rift zones of Kilauea and Mauna Loa obtained from time-dependent model. The bars represent 95% confidence intervals. The vertical gray bars mark the time of the 2005 silent slip event and June 2007 Kilauea east rift intrusion. The top panel shows the model results for Kilauea's magma chamber and rift zone and the bottom panel compares the volume changes of Kilauea and Mauna Loa magma chambers in Figure 3a. (b) Spatiotemporal frequency of >20 km deep seismicity and (c) time series of CO_2 emissions at Kilauea summit [*Poland et al.*, 2012]. The yellow transparent rectangle spans the duration of the 2004 deep seismicity pulse.

trend of the deformation. The temporal pattern of the inferred volume change of Mauna Loa's magma chamber is similar to that of Kilauea's rift and also shifts its relation to Kilauea's magma chamber from anticorrelation to correlation, in late 2005.

[16] During the second half of 2004, deep seismicity (>20 km) below Mauna Loa's summit caldera increased significantly (Figures 3b, S7a, and S7c). This coincides with measurements of elevated CO_2 emissions at the Kilauea summit (Figure 3c), indicating increased magma supply to

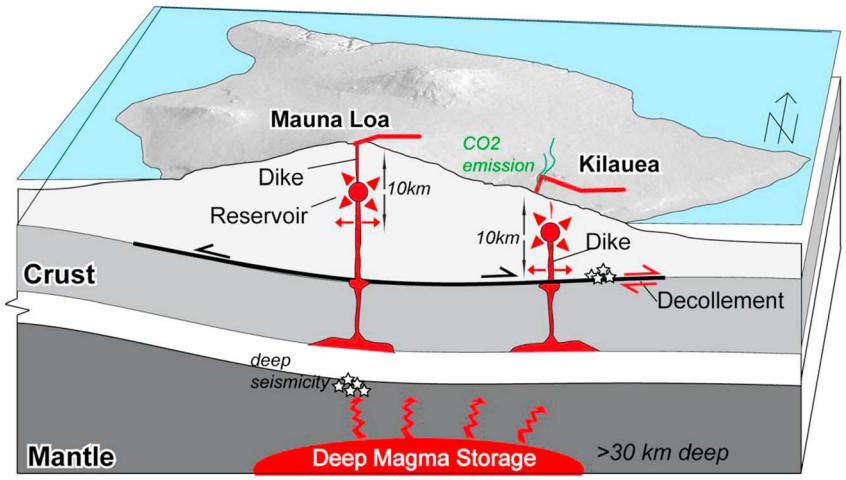

Figure 4. Cartoon illustrating magmatic and deformation processes on Hawaii during 2003–2008. A mantle-driven surge increased the supply to both systems and caused rift intrusion at Kilauea and magma chamber inflation at both volcanoes. The deep intrusions into Kilauea's rift zone may also have triggered the 2005 silent slip event. The reason for different magma compositions at Kilauea and Mauna Loa may be due to the different magma travel paths along which interaction with host rock alters the chemical makeup of the extruded lava. Figure redrawn and updated from *Walter and Amelung* [2006].

Kilauea from a source within the mantle [*Poland et al*., 2012]. The cartoon of Figure 4 summarizes the processes associated with deformation and seismicity on Hawaii, during 2003–2008. The surge of magma supply from the deep mantle affected both Kilauea and Mauna Loa and caused simultaneous deformation rate changes (Figures 1 and S2). The elevated deep seismicity under Mauna Loa and enhanced CO_2 emissions at Kilauea at the end of 2004 suggest that the surge accelerated during the second half of 2004 leading to enhanced magma supply to Mauna Loa's and Kilauea's magmatic systems, possibly by pore pressure diffusion in a common, asthenospheric magma supply system [*Gonnermann et al*., 2012]. We propose that this is why Mauna Loa's magma chamber and Kilauea's rift zone show very similar temporal behavior during this episode. The rift opening and intrusions during 2004 may have triggered the January 2005 SSE on Kilauea's south flank décollement [*Brooks et al*., 2008; *Cayol et al*., 2000; *Dieterich et al*., 2000]. The ongoing surge continued to dominate the deformation at both Mauna Loa and Kilauea as evidenced in the correlated behavior during the years after the 2005 SSE. Occasional short-term anticorrelations are observed between Kilauea's rift zone and magma chamber due to the transport of magma from the summit chamber to the rift vents [*Poland et al*., 2012].

[17] The data and models presented in this study reveal that the condition for correlated behavior of the Hawaiian volcanoes lies in the mantle-driven surge of magma supplied to both Mauna Loa and Kilauea. This also explains why during the 1984 Mauna Loa eruption no substantial deformation was observed at Kilauea [*Delaney et al*., 1998]. Given the steady rate of the supply to the volcanic systems for the previous few decades [*Poland et al*., 2012], the 1984 event likely was related to a preexisting magma body trapped at shallower levels and not to a major mantle-driven surge. This event was not accompanied by deep seismicity (Figure S7c), and only shallow elevated microseismicity occurred at 5–13 km [*Lockwood et al*., 1985], the depth at which most of Mauna Loa's deep rift intrusions take place.

[18] Several times over the last 2000 years, Kilauea has erupted lavas with composition similar to that of Mauna Loa as reported by *Rhodes et al*. [1989]. They also suggest that occasionally the Kilauea magmatic pluming system is invaded by Mauna Loa magma. Thus, we speculate that this invasion likely occurs during deep mantle surges. Here we showed that following a deep-seated mantle surge, strong coupling between Mauna Loa and Kilauea initiated in 2005. Likely, such correlated behavior only occurs when Kilauea's plumbing system is invaded by Mauna Loa magma.

[19] **Acknowledgments.** The interferograms used in this study were generated using the GMTSAR software [*Sandwell et al*., 2011]. Radar data were provided by the European Space Agency under project C1P-9539 and C1P-1354. We thank Paul Lundgren and an anonymous reviewer for their helpful reviews.

[20] The Editor thanks Paul Lundgren and an anonymous reviewer for their assistance in evaluating this paper.

References

Amelung, F., S. H. Yun, T. R. Walter, P. Segall, and S. W. Kim (2007), Stress control of deep rift intrusion at Mauna Loa volcano, Hawaii, *Science*, *316*, 1026–1030.

Baker, S., and F. Amelung (2012), Top-down inflation and deflation at the summit of Kilauea Volcano, Hawai`i observed with InSAR, *J. Geophys. Res.*, *117*, B12406, doi:10.1029/2011JB009123.

Bjerhammar, A. (1973), *Theory of Errors and Generalized Matrix Inverse*, Elsevier publishing company, Amsterdam, pp. 127–128.

Brooks, B. A., J. Foster, D. Sandwell, C. J. Wolfe, P. Okubo, M. Poland, and D. Myer (2008), Magmatically triggered slow slip at Kilauea Volcano, Hawaii, *Science*, *321*(5893), 1177.

Cayol, V., J. H. Dieterich, A. T. Okamura, and A. Miklius (2000), High magma storage rates before the 1983 eruption of Kilauea, Hawaii, *Science*, *288*(2343).

Chen, C. W., and H. A. Zebker (2001), Two-dimensional phase unwrapping with use of statistical models for cost functions in nonlinear optimization, *J. Opt. Soc. Am. A*, *18*, 338–351.

Costantini, M., and P. A. Rosen (1999), A generalized phase unwrapping approach for sparse data, paper presented at Proceedings of the IEEE 1999 International Geoscience and Remote Sensing Symposium (IGARSS), Hamburg.

Delaney, P. T., R. Denlinger, M. Lisowski, A. Miklius, P. Okubo, A. Okamura, and M. K. Sako (1998), Volcanics spreading at Kilauea, 1976–1996, *J. Geophys. Res.*, *103*(B8), 18003–18023.

Desmarais, E. K., and P. Segall (2007), Transient deformation following the 30 January 1997 dike intrusion at Kilauea volcano, Hawai`i, *Bull. Volcanol.*, *69*(4), 353–363.

Dieterich, J., V. Cayol, and P. Okubo (2000), The use of earthquake rate changes as a stress meter at Kilauea volcano, *Nature*, *408*(6811), 457.

Franceschetti, G., and R. Lanari (1999), *Synthetic Aperture Radar Processing*, CRC Press, Boca Raton, FL.

Fujii, T., and I. Kushiro (1977), Density, viscosity, and compressibility of basaltic liquid at high pressures, in Annual Report of the Director 1976–1977 Rep., pp. 419–424 , Geophysical Laboratory, Carnegie Institution, Washington, D. C.

Gonnermann, H. M., J. H. Foster, M. Poland, C. J. Wolfe, B. A. Brooks, and A. Miklius (2012), Coupling at Mauna Loa and Kılauea by stress transfer in an asthenospheric melt layer, *Nat. Geosci*, doi:10.1038/ngeo1612.

Grewal, M. S., and A. P. Andrews (2001), *Kalman Filtering: Theory and Practice Using MATLAB*, Wiley-Interscience, New York, pp. 416.

Hill, D. P., F. Pollitz, and C. Newhall (2002), Earthquake-volcano interactions, *Phys. Today*, *55*(11), 41–47.

Houghton, B., H. Rymer, J. Stix, S. McNutt, and H. Sigurdsson (1999), *Encyclopedia of Volcanoes*, Academic Press, San Diego, pp. 1417.

Klein, F. W. (1982), Patterns of historical eruptions at Hawaiian volcanoes, *J. Volcanol. Geotherm. Res.*, *12*, 1–35.

Linde, A. T., and I. S. Sacks (1998), Triggering of volcanic eruptions, *Nature*, *395*(6705), 888–890.

Lockwood, J. P., N. G. Banks, T. T. English, L. P. Greenland, D. B. Jackson, D. J. Johnson, R. Y. Koyanagi, K. A. McGee, A. T. Okamura, and J. M. Rhodes (1985), The 1984 eruption of Mauna Loa Volcano, Hawaii, *Eos Trans. AGU*, *66*(16), 169–171.

Manga, M., and E. Brodsky (2006), Seismic triggering of eruptions in the far field: Volcanoes and geysers, *Ann. Rev. Earth Planet. Sci.*, *34*, 263–291, doi:10.1146/annurev.earth.34.031405.125125.

Massonnet, D., M. Rossi, C. Carmona, F. Adragna, G. Peltzer, K. Feigl, and T. Rabaute (1993), The displacement field of the Landers earthquake mapped by radar interferometry, *Nature*, *364*, 138–142.

McTigue, D. F. (1987), Elastic stress and deformation near a finite spherical magma body: Resolution of the point source paradox, *J. Geophys. Res.*, *92*, 12931–12940.

Miklius, A., and P. Cervelli (2003), Interaction between Kilauea and Mauna Loa, *Nature*, *421*, 229.

Montgomery-Brown, E. K., P. Segall, and A. Miklius (2009), Kilauea slow slip events: Identification, source inversions, and relation to seismicity, *J. Geophys. Res.-Sol. Ea.*, *114*, B00A03, doi:10.1029/2008JB006074.

Montgomery-Brown, E. K., D. Sinnett, M. Poland, P. Segall, T. Orr, H. Zebker, and A. Miklius (2010), Geodetic evidence for en echelon dike emplacement and concurrent slow slip during the June 2007 intrusion and eruption at Kīlauea volcano, Hawaii, *J. Geophys. Res.*, *115*, B07405, doi:10.1029/2009JB006658.

Montgomery-Brown, E. K., D. K. Sinnett, K. M. Larson, M. P. Poland, P. Segall, and A. Miklius (2011), Spatiotemporal evolution of dike opening and decollement slip at Kilauea Volcano, Hawai`i, *J. Geophys. Res.-Sol. Ea.*, *116*, B03401, doi:10.1029/2010JB007762.

Moore, J. G. (2001), Density of basalt core from Hilo drill hole, Hawaii, *J. Volcanol. Geotherm. Res.*, *112*(1–4), 221–230, doi:10.1016/s0377-0273(01)00242-6.

Myer, D., D. Sandwell, B. Brooks, J. Foster, and M. Shimada (2008), Inflation along Kilauea's southwest rift zone in 2006, *J. Volcanol. Geotherm. Res.*, *177*(2), 418–424.

Okada, Y. (1985), Surface deformation due to shear and tensile faults in a half-space, *Bull. Seism. Soc. Am.*, *75*, 1135–1154.

Okubo, P. G., H. M. Benz, and B. A. Chouet (1997), Imaging the crustal magma sources beneath Mauna Loa and Kilauea volcanoes, Hawaii, *Geology 25*(10), 867–870.

Owen, S., P. Segall, M. Lisowski, A. Miklius, R. Denlinger, and M. Sako (2000), Rapid deformation of Kilauea Volcano: Global Positioning System measurements between 1990 and 1996, *J. Geophys. Res.*, *105*(B8), 18,983–918,998.

Poland, M. P., A. Miklius, A. J. Sutton, and C. R. Thornber (2012), A mantle-driven surge in magma supply to Kīlauea Volcano during 2003–2007, *Nat. Geosci.*, *5*, 295–300.

Rhodes, J. M., K. P. Wenz, C. A. Neal, J. W. Sparks, and J. P. Lockwood (1989), Geochemical evidence for invasion of Kilauea's plumbing system by Mauna Loa magma, *Nature*, *337*(6204), 257–260.

Sandwell, D., R. Mellors, X. Tong, M. Wei, and P. Wessel (2011), Open radar interferometry software for mapping surface deformation, *Eos Trans. AGU*, *92*(28), doi:10.1029/2011EO280002.

Segall, P., E. K. Desmarais, D. Shelly, A. Miklius, and P. Cervelli (2006), Earthquakes triggered by silent slip events on Kılauea volcano, Hawaii, *Nature*, *442*(7098), 71–74, doi:10.1038/nature04938.

Shirzaei, M. (2013), A wavelet-based multitemporal DInSAR algorithm for monitoring ground surface motion, *IEEE Geosci. Remote Sens. Lett.*, *10*(3), 456–460, doi:10.1109/Lgrs.2012.2208935.

Shirzaei, M., and R. Bürgmann (2012), Topography correlated atmospheric delay correction in radar interferometry using wavelet transforms, *Geophys. Res. Lett.*, *39*(1), L01305, doi:10.1029/2011GL049971.

Shirzaei, M., and T. R. Walter (2009), Randomly iterated search and statistical competency (RISC) as powerful inversion tools for deformation source modeling: Application to volcano InSAR data, *J. Geophys. Res.*, *114*, B10401, doi:10.1029/2008JB006071.

Shirzaei, M., and T. R. Walter (2010), Time-dependent volcano source monitoring using interferometric synthetic aperture radar time series: A combined genetic algorithm and Kalman filter approach, *J. Geophys. Res.*, *115*, B10421, doi:10.1029/2010JB007476.

Shirzaei, M., and T. R. Walter (2011), Estimating the effect of satellite orbital error using wavelet based robust regression applied to InSAR deformation data, *IEEE Trans. Geosci. Remote Sens.*, *49*(1), 4600–4605.

Siebert, L., T. Simkin, and P. Kimberly (2010), *Volcanoes of the World*, University of California Press, Berkeley, pp. 551 .

Sigmundsson, F., H. Vadon, and D. Massonnet (1997), Readjustment of the Krafla spreading segment to crustal rifting measured by satellite radar interferometry, *Geophys. Res. Lett.*, *24*(15), 1843–1846.

Walter, T. R., and F. Amelung (2006), Volcano-earthquake interaction at Mauna Loa volcano, Hawaii, *J. Geophys. Res.*, *111*(B05204), doi:10.1029/2005JB003861.